AEDC-TR-76-54

(12)

ADA033116

MEASUREMENT AND MAPPING OF AERODYNAMIC
HEATING IN VKF TUNNEL B WITH
AN INFRARED CAMERA

VON KÁRMÁN GAS DYNAMICS FACILITY
ARNOLD ENGINEERING DEVELOPMENT CENTER
AIR FORCE SYSTEMS COMMAND
ARNOLD AIR FORCE STATION, TENNESSEE 37389

November 1976

Interim Report for Period July 1, 1973 — June 30, 1975

D D C
DEC 7 1976
C

Prepared for

DIRECTORATE OF TECHNOLOGY (DY)
ARNOLD ENGINEERING DEVELOPMENT CENTER
ARNOLD AIR FORCE STATION, TENNESSEE 37389

This report has been reviewed by the Information Office (OI) and is releasable to the National Technical Information Service (NTIS). At NTIS, it will be available to the general public, including foreign nations.

APPROVAL STATEMENT

This technical report has been reviewed and is approved for publication.

FOR THE COMMANDER

MARSHALL K. KINGERY
Research & Development
  Division
Directorate of Technology

ROBERT O. DIETZ
Director of Technology

UNCLASSIFIED

REPORT DOCUMENTATION PAGE		READ INSTRUCTIONS BEFORE COMPLETING FORM
1. REPORT NUMBER AEDC-TR-76-54	2. GOVT ACCESSION NO.	3. RECIPIENT'S CATALOG NUMBER
4. TITLE (and Subtitle) MEASUREMENT AND MAPPING OF AERODYNAMIC HEATING IN VKF TUNNEL B WITH AN INFRARED CAMERA.		5. TYPE OF REPORT & PERIOD COVERED Final Report. 1 Jul 1, 1973-30 June 1975,
		6. PERFORMING ORG. REPORT NUMBER
7. AUTHOR(s) D. S. Bynum, F. K. Hube, C. M. Key and P. M. Dyer, ARO, Inc.		8. CONTRACT OR GRANT NUMBER(s)
9. PERFORMING ORGANIZATION NAME AND ADDRESS Arnold Engineering Development Center (DY) Air Force Systems Command Arnold Air Force Station, Tennessee 37389		10. PROGRAM ELEMENT, PROJECT, TASK AREA & WORK UNIT NUMBERS Program Element 65807F
11. CONTROLLING OFFICE NAME AND ADDRESS Arnold Engineering Development Center (DYFS) Arnold Air Force Station, Tennessee 37389		12. REPORT DATE November 1976
		13. NUMBER OF PAGES 33
14. MONITORING AGENCY NAME & ADDRESS(if different from Controlling Office) 36p.		15. SECURITY CLASS. (of this report) UNCLASSIFIED
		15a. DECLASSIFICATION DOWNGRADING SCHEDULE N/A

16. DISTRIBUTION STATEMENT (of this Report)

Approved for public release; distribution unlimited.

17. DISTRIBUTION STATEMENT (of the abstract entered in Block 20, if different from Report)

18. SUPPLEMENTARY NOTES

Available in DDC

19. KEY WORDS (Continue on reverse side if necessary and identify by block number)

heat transfer	angle of attack
data acquisition	Mach number
conical bodies	Reynolds numbers
hemispheres (cylinder)	infrared scanning camera

20. ABSTRACT (Continue on reverse side if necessary and identify by block number)

Heat-transfer data were obtained on a cone and a hemisphere-cylinder model using an infrared scanning camera. Data were obtained at Mach number 8 at free-stream Reynolds numbers ranging from 2.4 x 10⁶ to 3.5 x 10⁶ per foot and all tests were conducted at zero angle of attack. Runs with the cone were made with and without a boundary-layer trip to produce a variation → next page

2,400,000   3,500,000

DD FORM 1473 1 JAN 73   EDITION OF 1 NOV 65 IS OBSOLETE

UNCLASSIFIED   042 550

20. ABSTRACT (Continued)

cont. in the heating distributions measured with the camera. Data compare favorably with theoretical heating levels and distributions.

AFSC
Arnold AFS Tenn

PREFACE

The work reported herein was conducted by the Arnold Engineering Development Center (AEDC), Air Force Systems Command (AFSC), under Program Element 65807F. The results were obtained by ARO, Inc. (a subsidiary of Sverdrup & Parcel and Associates, Inc.), contract operator of AEDC, AFSC, Arnold Air Force Station, Tennessee. The research program was conducted under ARO Project No. V32S-22A and some later, additional experimental data were acquired as part of ARO Project No. V41B-B1A. The authors of this report were D. S. Bynum, F. K. Hube, C. M. Key, and P. M. Dyer, ARO, Inc. The manuscript (ARO Control No. ARO-VKF-TR-75-152) was submitted for publication on October 15, 1975.

CONTENTS

ILLUSTRATIONS

AEDC-TR-76-54

4

1.0 INTRODUCTION

Measuring and mapping aerodynamic heating parameters in the Arnold Engineering Development Center (AEDC)-von Kármán Gas Dynamics Facility (VKF) continuous wind tunnels have been accomplished by a variety of techniques (Ref. 1). Measurement of discrete spatial values of heating has been done using thin-skin models with back surface thermocouples and thick-walled models with Gardon gages and surface thermocouples. Mapping has been accomplished with heat sensitive paints, both phase change and phosphorescent (Refs. 2 and 3). Though not original with the AEDC, the previously mentioned techniques have been refined and adapted to the AEDC-VKF continuous wind tunnels. The data from gages and thermocouples are amenable to automatic data reduction by analog-to-digital conversion equipment and digital computers and thus can yield online data useful for test direction and data monitoring purposes. However, there are generally insufficient points on the model to satisfactorily map the heating parameters. The temperature-sensitive paints can map heating parameters, but at their present state of development require weeks of subsequent analysis to obtain reduced data.

An infrared (IR) scanning camera system can map heating parameters and its data can be reduced automatically online, thus incorporating a principal advantage of each of the previously mentioned techniques. Several investigators, both in the United States and in Europe, have applied the IR technique to measuring and mapping aerodynamic heating parameters (Refs. 4 through 7). The AEDC-VKF recognized the potential of the technique and is pursuing its refinement and adaption to the more rapid production and fast turnaround of data required to fully utilize the testing characteristics of the VKF continuous wind tunnels.

This report gives a description of the IR system used to acquire and reduce the heating data and the results of the first measurement and mapping of aerodynamic heating parameters in AEDC-VKF wind tunnels using this technique. One-dimensional heat flow in a semi-infinite solid was selected as the mechanism to transduce aerodynamic heating into surface temperature. This transducing scheme has been proven valid both by analysis and experiment for use with temperature-sensitive paint and surface thermocouples. The surface temperature of the model in the present work was measured with the IR system. The IR surface temperature measurement could also be applied to thin-skin models.

5

Because the emphasis was on acquiring quantitative data and not online data reduction, it was deemed expedient to use an offline data digitizing and reducing system built mostly from components on hand in the VKF. To fully realize the online data potential of the technique, an automated direct-digitizing and recording system is planned and is expected to be operational in late FY 77.

A 6-in.-diam hemisphere cylinder and a 6-deg half-angle blunted cone with a 0.2-in. nose radius were tested in Hypersonic Wind Tunnel (B) (Tunnel B) at Mach 8 and the results compared with theory to evaluate the quantitative data capability of the IR system.

2.0 APPARATUS

2.1 MODELS

The models used for this test were a 6-deg half-angle blunted cone with a 0.2-in. nose radius and a 6-in.-diam hemisphere-cylinder. The geometry of these models is shown in Figs. 1 and 2, respectively, and model photographs are presented in Figs. 3 and 4. Both models are constructed with an RTV-60® skin nominally 0.250 in. thick supported by a metal core. The cone model has a metal nosetip for structural integrity and a protruding rod (Fig. 5) to generate high heating gradients to evaluate the mapping capability of the IR technique under such conditions. A boundary-layer trip shown in Figs. 1 and 6 was used when turbulent boundary layer was desired.

The emissivity of the RTV-60 which is required for data reduction was determined by reflectance measurements to be 0.8 in the spectral range of the camera.

2.2 TUNNEL B

Tunnel B is a closed-circuit, continuous flow wind tunnel with variable density capability. It has axisymmetric nozzles for Mach numbers 6 and 8, both with 50-in.-diam test sections. The stagnation pressure is variable from 20 to 300 psia and from 50 to 900 psia, respectively, for the low and high Mach numbers. Maximum stagnation temperature is 1,350°R. More details of Tunnel B can be found in Ref. 8.

The models (Section 2.1) and the IR camera (Section 2.3.1) were installed in Tunnel B as shown in Fig. 7.

6
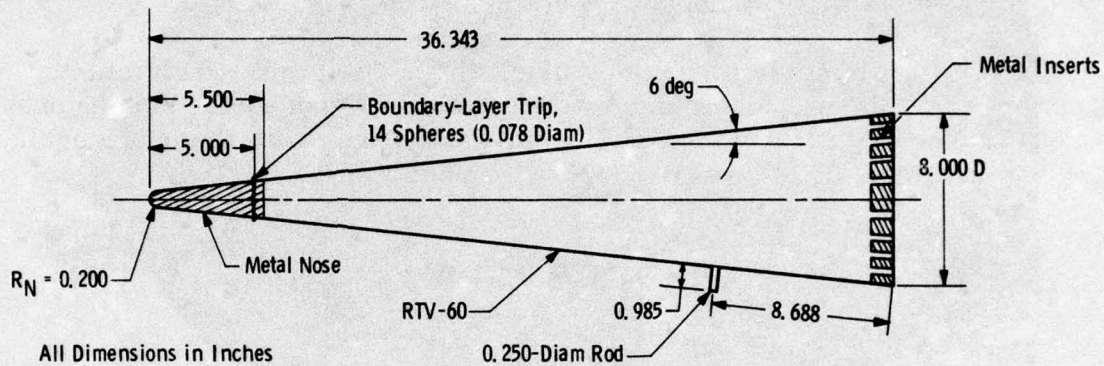
Figure 1. Cone model geometry.

All Dimensions in Inches
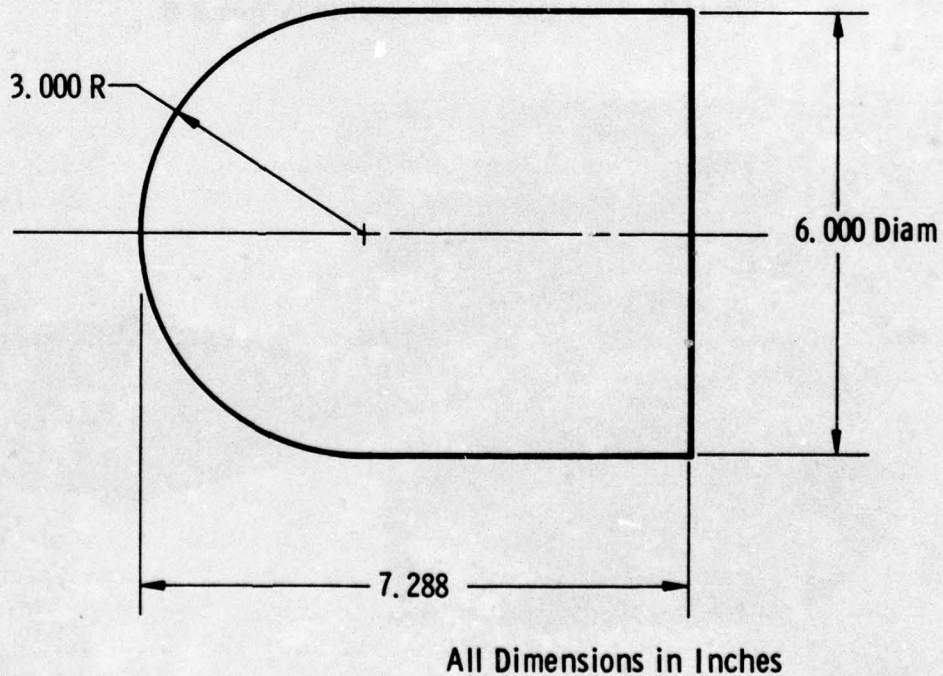
Figure 2. Hemisphere-cylinder model.

7
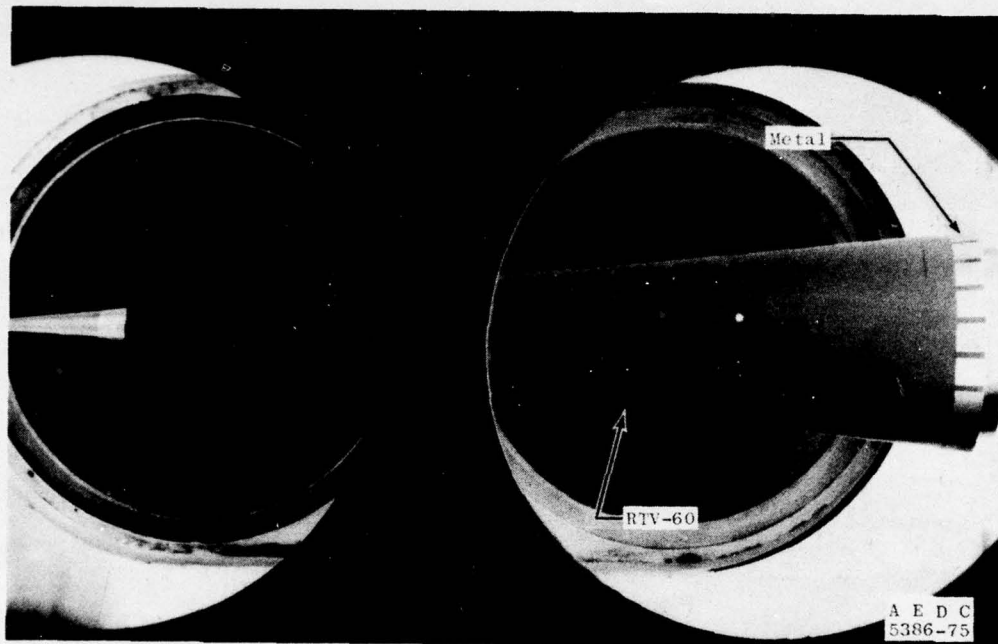
Figure 3. 6-deg cone model installed in Tunnel B.
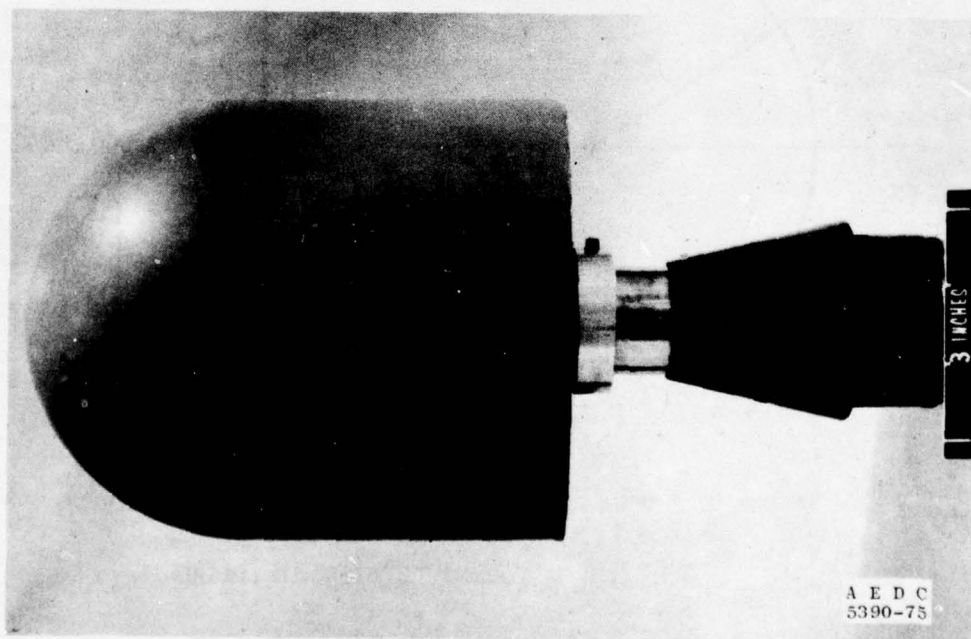
Figure 4. 3-in.-radius hemisphere-cylinder model.
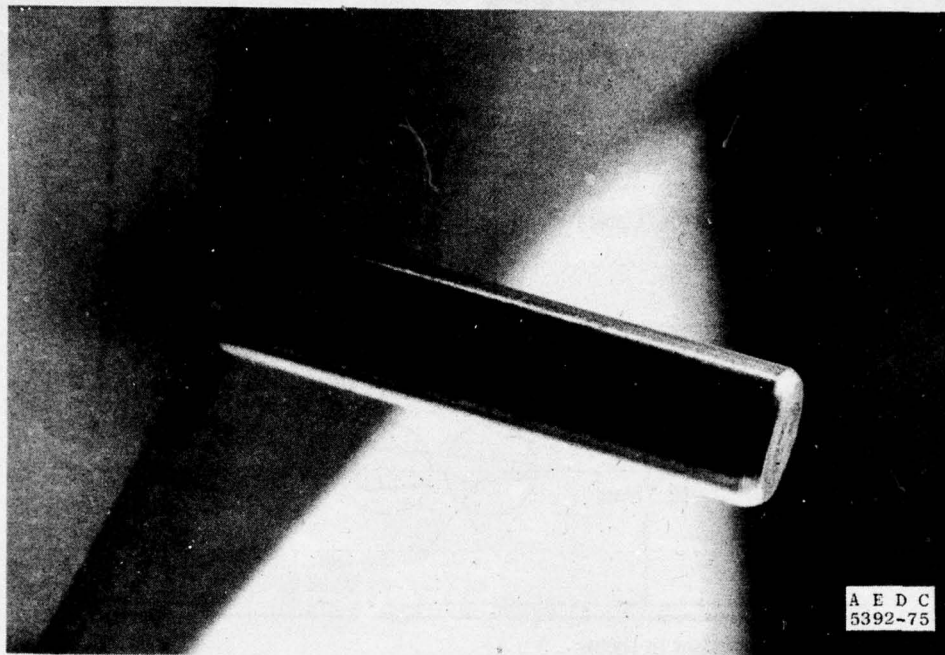
Figure 5. Protruding rod on 6-deg cone model.
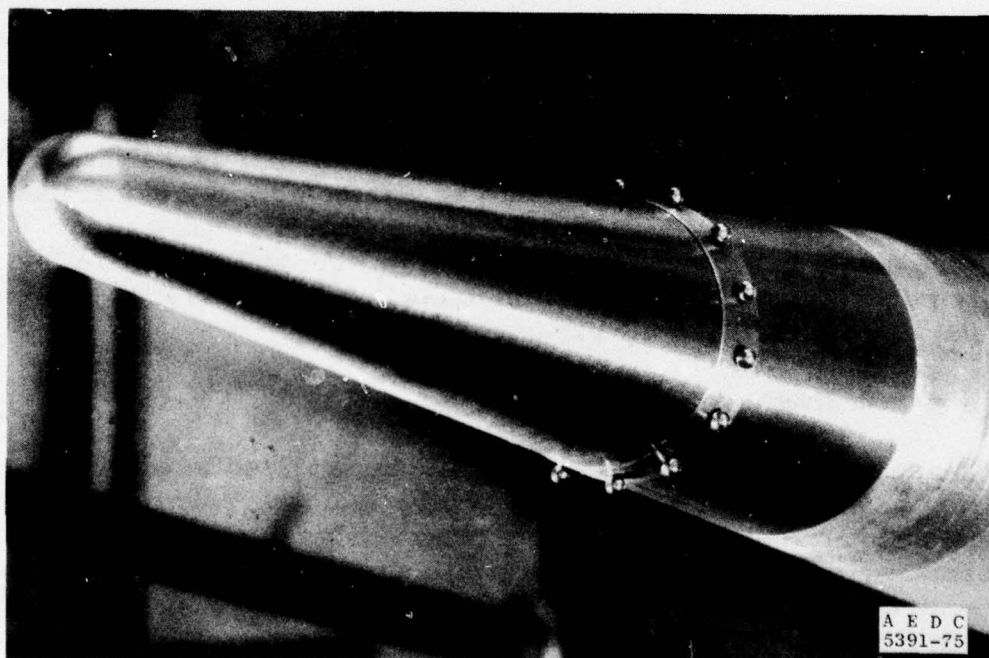
Figure 6. Boundary-layer trip on 6-deg cone model.
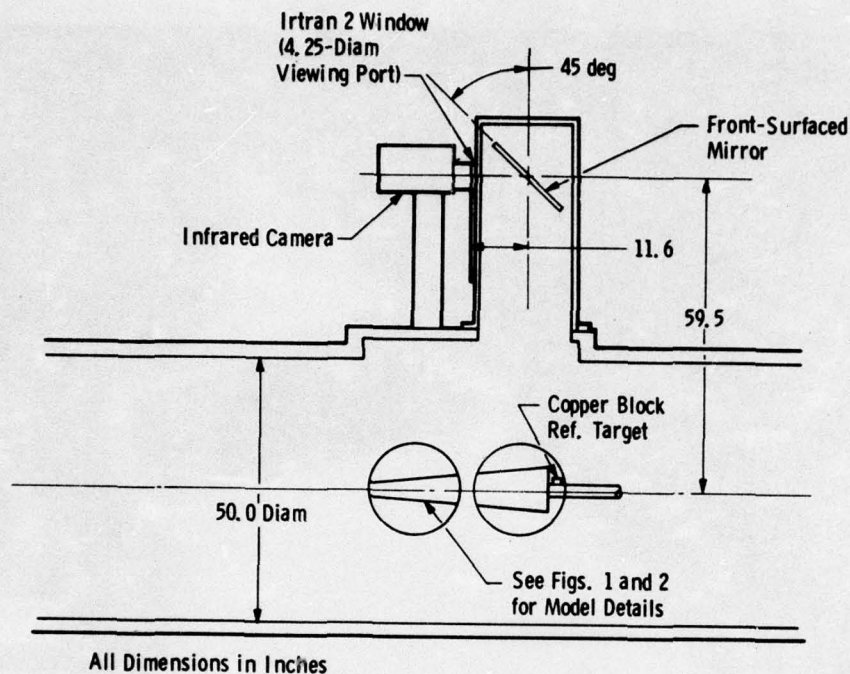
Figure 7. Model and camera installation in Tunnel B.

2.3 INFRARED SYSTEM

Block diagrams of the instrumentation systems used to obtain model surface temperature data are shown in Figs. 8 and 9. IR radiation emitted by the model is converted into an electronic video signal that is displayed on the monitors and recorded on analog magnetic tape. The video signal is replayed from the tape system and digitized providing digitized data for computer reduction to obtain model surface temperature and aerodynamic heating parameters.

2.3.1 IR Camera System

Components of the AGA Model 680 IR camera used to convert IR radiation into electronic video signal are two rotating prisms for vertical and horizontal scanning, two prism-drive motors, prism position sensors, collimating lens, chopper assembly, IR detector, and a liquid-nitrogen dewar as shown in Fig. 10. An optical schematic is shown in Fig. 11.
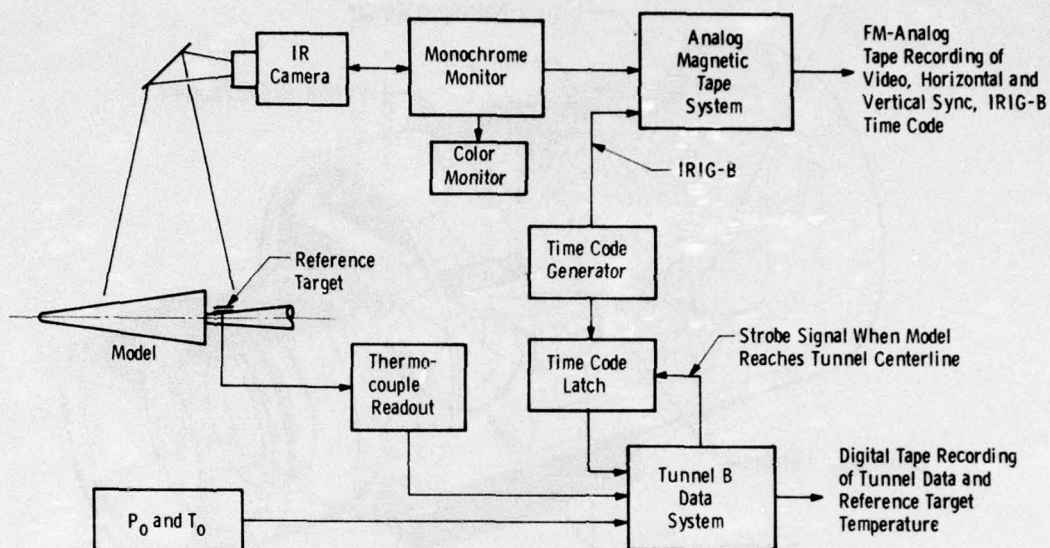
Figure 8. Data recording system.
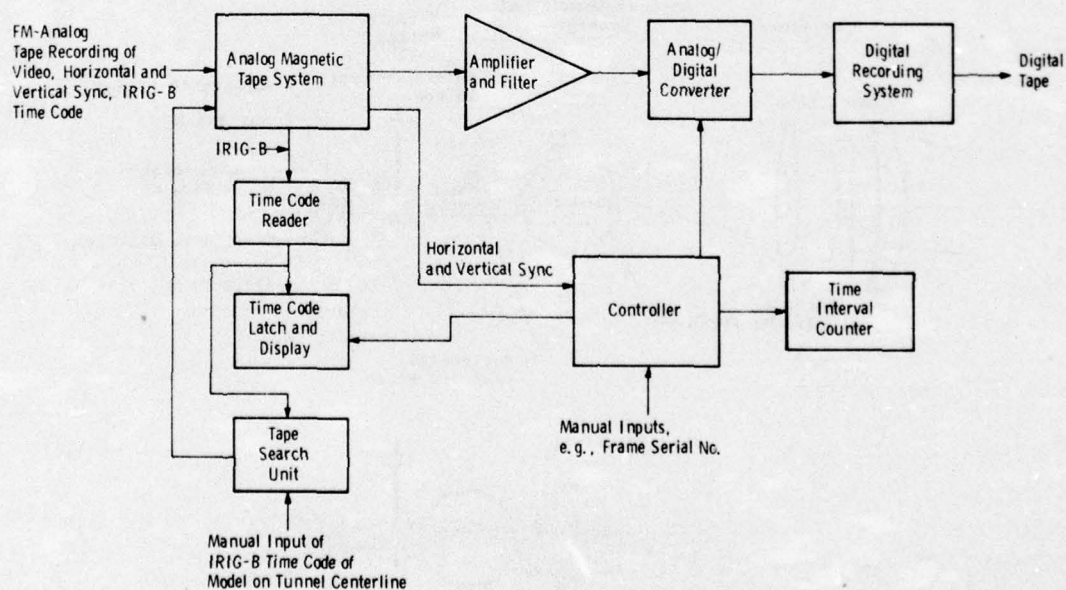
Figure 9. Data digitizing system.

11
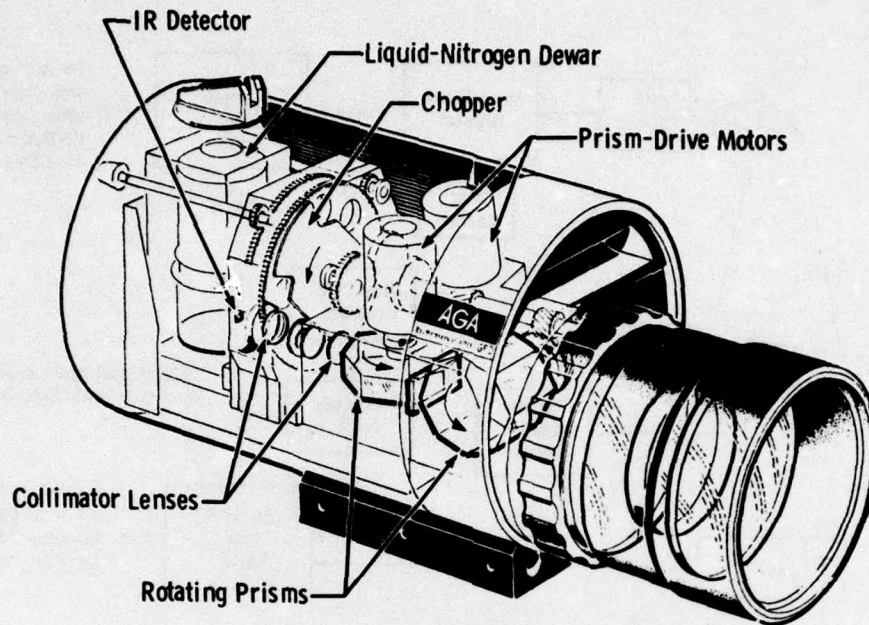
Figure 10. Infrared camera unit.
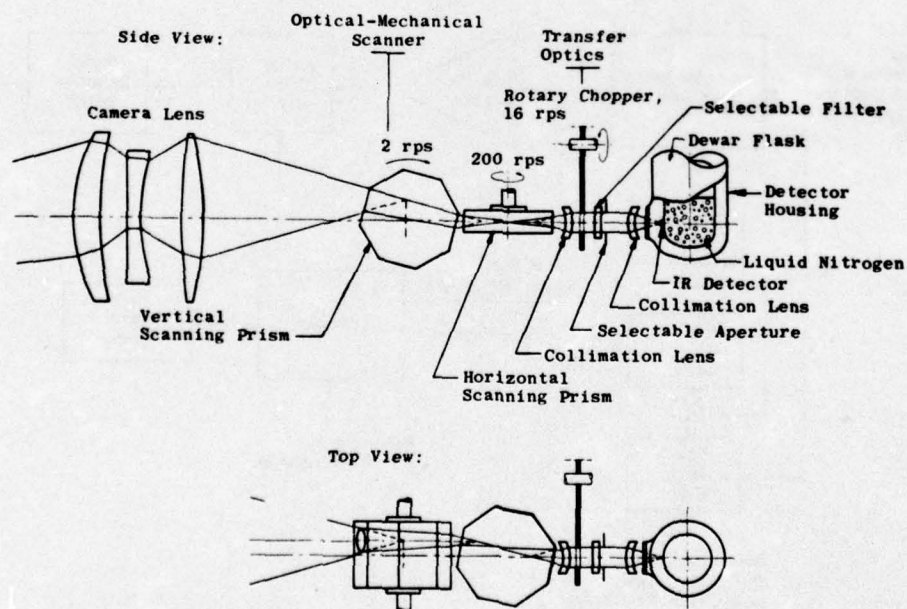
Figure 11. Optical schematic of the infrared camera.

12

Scanning of the viewed object is accomplished with the two prisms. A virtual image of the model is formed by the front lens of the camera on a plane within the first prism. Vertical scanning is accomplished by rotating the first prism about its horizontal axis and horizontal scanning is achieved by rotating the second prism at a faster speed about its vertical axis. Vertical scan rate is 16 fields or frames per second. Speed relationship of the two prisms is regulated at approximately 100 horizontal scans in one vertical scan. This provides random interlaced scanning to improve the appearance of scenes viewed on the monitors. The two prisms are not phase-locked, thus their phase relationship is allowed to change gradually. The effect of this is to raise or lower the scanned field a fraction of a scanning-line width on successive vertical scans. This feature of the camera has not been used so far to improve the mapping detail of the digital data. An aluminum chopper rotates in synchronism with the vertical scanner, chopping off the IR beam to the detector during approximately 20 percent of the scanning period. The polished aluminum chopper blade functions as a temperature reference since it reflects an image of the cooled detector back on itself.

The IR-sensitive detector in the camera is an indium antimonide photovoltaic cell sensitive to the 2- to 5-μ wavelength band. The detector is mounted in the liquid-nitrogen dewar to obtain the required performance. A single filling of the dewar lasts approximately four hours.

Radiant flux from the scanner impinging on the detector generates an electrical voltage signal across the terminals of the detector. Amplitude of the signal varies according to the temperature variations along the surface of the object as it is being scanned by the camera. The electrical signal is amplified by a video preamplifier and a sensitivity control amplifier, both direct-coupled to retain the signal component which represents the absolute temperature level being sensed by the detector.

The monochrome monitor provides the controls for adjusting the d-c component and the sensitivity of the camera video signal. The video signal recorded on analog magnetic tape was obtained from the output of the monochrome monitor sensitivity control amplifier.

The color monitor provides a visual display in which color bands represent ranges of temperature. Thus, the boundary between two colors is an isotherm.

2.3.2 Analog Magnetic Tape System

A Bell and Howell Model VR-3700B analog magnetic tape system was used for recording the IR camera signals. The FM mode of recording was used and tape speed was 120 ips. Bandwidth for the tape system at this speed and mode of recording is DC to 500 kHz. Bandwidth of the video data from the IR camera was DC to 100 kHz.

Four signals (vertical sync, horizontal sync, video, and IRIG-B time code) were recorded on tape. The vertical and horizontal sync signals were used during replay of the data to control when the video signal was digitized and to obtain the time for each vertical scan and the random-interlace timing. The time code signal was used to control the operation of the tape system during replay and provide a readout of time for the digitized frame.

Replay of the IR camera data was at a tape speed of 3-3/4 ips providing a digitizing rate reduction by a factor of 32. Sampling rate for the video replay signal was 7.8125 kHz. The tape search unit controls the tape transport mechanism during search and playback operation. To locate a given block of data on tape, a start and stop time is selected and these values are compared to the time code signal recorded on tape. Tape transport will drive in the correct direction at 120 ips until the start time is reached. When start time is reached, the tape transport mechanism will reverse direction and go beyond start time in reverse to a predetermined time. At this time the tape transport will stop and reverse direction again, approaching start time at a speed of 3-3/4 ips. At the value of start time, a control signal is generated to enable the digitizing of the video signal. Any field or frame of the video signal can be digitized automatically on the basis of previously known recorded time. Resolution of the time code reader and comparator is 1 msec.

2.3.3 Analog-to-Digital Converter Controller

Selection of which frame and how many points within a frame to digitize is determined with the analog-to-digital converter (ADC) controller. Thumbwheel switches allow selection of which frame after a certain time, how many lines within a frame, and how many points within a line. A maximum of approximately 70 lines and 99 points per line can be digitized. One field or any number of successive fields can be digitized.

14

Four control signals are obtained from the controller as follows:

1. Take data strobe for the ADC,

2. Strobe to latch digital output of time code reader into a register for the digitized frame,

3. Two pulses for measuring time interval between vertical sync and first horizontal line sync pulse, and

4. Light-up pulses for intensity modulation of the beam of the monochrome monitor.

The light-up pulses are used in real time to determine the location of objects in the scanned picture and to determine the X-Y distance resolution of the digitized points.

2.3.4 Analog-to-Digital Converter

Analog voltages (full scale to ±10 volts) are converted to 15 bit binary words. Specifications of the converter are as follows:

Input range - ±10 v

Voltage resolution - approximately 0.61 mv/count

Aperture - 50 nsec

Throughput rate - 40 kHz maximum

2.3.5 Digital Recording System

The digital data from the ADC was stored on the disc unit of a DEC PDP-11/40 computer and then transferred from the disc to magnetic tape through a CDC 160-A computer.

2.4 REFERENCE TARGET

To circumvent the problems of measuring absolute radiation from the model surface, a differential radiation measurement was made. A reference radiation target was placed in the base region of the model. The target was copper plate (2 by 2 by 1/4 in.) mounted on the model support sting (see Fig. 7). The copper plate was painted to increase its emissivity. A pair of Chromel® -Alumel® thermocouples was bonded to the plate to measure the temperature. Emissivity of the plate (0.88) was measured in the laboratory with the AGA 680 IR

system. Location of the plate was determined by heating the plate and then intensifying the beam on the monochrome monitor at the corners of the plate. Line and point numbers were then recorded.

3.0 PROCEDURE

3.1 INFRARED SYSTEM CALIBRATION

Calibration of the IR camera was accomplished with a blackbody calibration source which has a conical cavity (7.83-deg half-angle) with approximately a 6-in. aperture. The source is heated by applying a variable voltage to a resistance heater, and temperature of the source is measured with a platinum resistance thermometer. Emissivity is equal to or greater than 0.99.

Calibration was accomplished with the camera mounted on Tunnel B as shown in Fig. 7. The blackbody radiation source previously des-cribed was mounted with the aperture on the centerline of the wind tunnel test section and approximately in the center of the field of view of the camera. The radiation from the source was viewed with the IR camera through all system optical components thus negating corrections for transmission and reflection losses. Magnitude of the IR radiation from the blackbody source was measured with the differential isothermal technique using the monochrome monitor.

Because the camera spectral response is essentially monochromatic (approximately 3.3 to 5.5 μ for the ten-percent amplitude response points), the calibration followed the form of Wein's approximation of Planck's radiation law.

$$I = K_1 e^{-K_2/T} \tag{1}$$

Therefore, the calibration data were plotted in terms of log of the isotherm units versus $1/T$, giving a straight line representation. A plot of the calibration is shown in Fig. 12.

A calibration of the camera was also made by directly viewing the conical cavity blackbody source. Combined transmission and reflec-tance losses of the window and mirror were determined from this calibration to be 0.09.
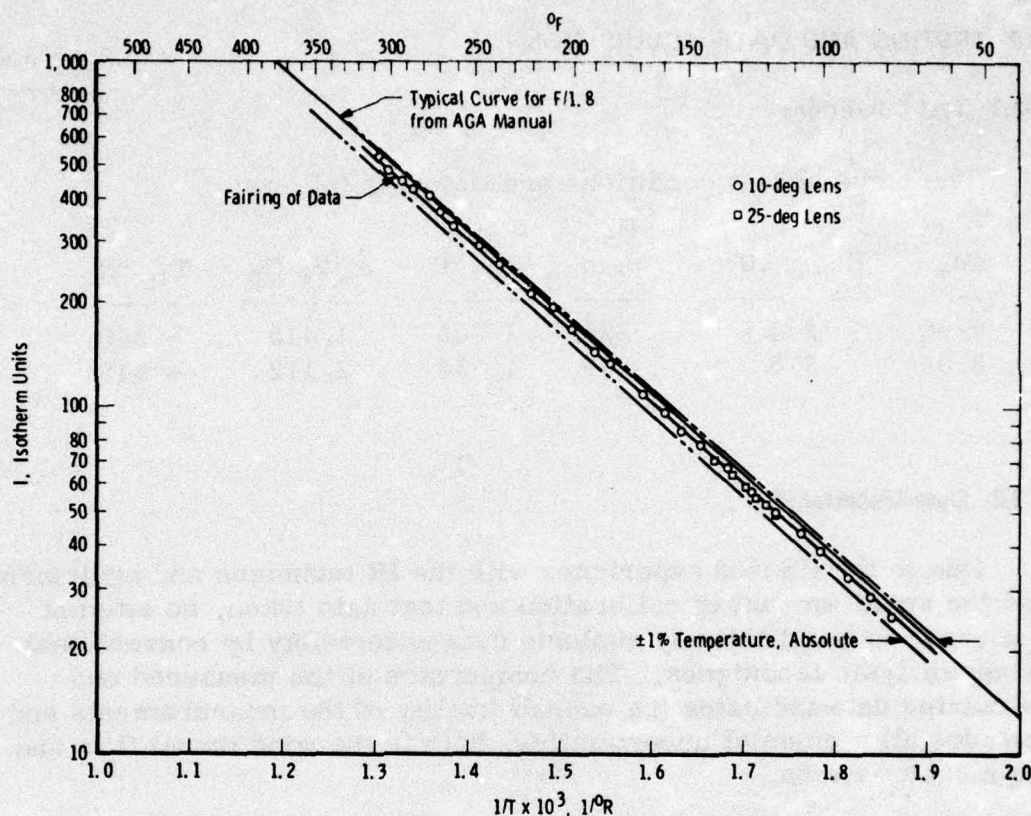
Figure 12. Camera calibration data.

Calibration of all instrumentation (tape machine, amplifier, and ADC) was accomplished by measuring the gain of each instrument for a known voltage input. A known voltage was recorded on the analog tape to serve as a calibration check during data replay.

The conversion factor for transforming isotherm units to volts or counts was determined by varying the reference level of video signal from the camera and digitizing the camera output signal.

17

3.2 TESTING AND DATA ACQUISITION

3.2.1 Test Conditions

The nominal test conditions are listed as follows:

M_∞	$Re_\infty \times 10^{-6}$	P_O, psia	T_O, °R	$\rho_\infty V_\infty C_p$	T_i, °R
7.98	2.4	520	1,305	1.415	~ 545
8.00	3.5	800	1,335	2.112	~ 545

3.2.2 Data Uncertainty

Due to the limited experience with the IR technique and equipment, and the small amount of calibration and test data taken, no attempt was made to quantitatively evaluate data uncertainty by conventional error analysis techniques. The comparison of the measured and calculated data indicates the overall quality of the measurements and includes all elemental uncertainties, both in the wind tunnel flow and the measurements.

3.2.3 Test Procedure

Both the cone and the hemisphere-cylinder model were tested at zero angle of attack. The model attitude was set with an inclinometer. Before injection of the model into the wind tunnel flow, the model initial temperature, T_i, was measured with a thermocouple pyrometer. Subsequent to each injection, the model was cooled to the desired T_i by flowing air over the model. The duration of the model exposure to the flow was limited by the maximum operating temperature (approximately 960°R) of the RTV-60 model surface. The model configurations tested with pertinent information are given below.

Configuration	M_∞	$Re_\infty \times 10^{-6}$	P_O, psia	T_O, °R	T_i, °R	Camera Field of View, deg
Cone	8.00	3.5	800	1,335	543	25
Cone with boundary-layer trip	8.00	3.5	800	1,335	546	25
Cone with boundary-layer trip	7.98	2.4	520	1,305	554	25
Cone with rod	8.00	3.5	800	1,335	544	25
Hemisphere-Cylinder	7.98	2.4	520	1,305	547	10

3.3 DATA REDUCTION

3.3.1 Basic Equation

The calculation of Stanton Number was based on a step application of the tunnel flow to the model, one-dimensional heat flow in the model, and on the stagnation temperature, T_o. The resulting equations are

$$St_\infty = \frac{h}{\rho_\infty V_\infty C_p} \tag{2}$$

$$\frac{T_w - T_i}{T_o - T_i} = 1 - e^{\beta^2} \text{erfc } \beta \tag{3}$$

where

$$\beta = \frac{h\sqrt{t}}{\sqrt{\rho ck}} \tag{4}$$

The IR system provided the raw data from which T_w was computed. A value of 0.24 Btu/lbm-°R was used for C_p and a value of 0.038 Btu/ft^2-°R-sec$^{1/2}$ was used for $\sqrt{\rho ck}$ for RTV-60. The time, t, is the elapsed time that the model has been exposed to the tunnel flow.

The equation for computation of T_w is

$$T_w = \frac{K_2}{\ln K_1 - \ln I_w} \tag{5}$$

where

$$I_w = \frac{\Delta i_{wr} + \epsilon_r I_r}{\epsilon_w} + (1 - \epsilon_r/\epsilon_w) I_a \tag{6}$$

The last term of Eq. (6) is the amount of thermal radiation reflected from the surroundings by the model. It is a difficult term to evaluate because an equivalent ambient temperature is not known. However, the ambient radiation is believed to be dominated by the water cooled portion of the tunnel test section. During this particular test entry, the cooling water temperature was approximately 540°R. Referring to the calibration data in Fig. 12, I_a equals approximately 25 isotherm units and when multiplied by $(1 - \epsilon_r/\epsilon_w)$ (which has a vlaue of 0.1) is equal to 2.5 isotherm units. This is negligible compared with even the lowest values of I_w (approximately 100 isotherm units) encountered during data reduction.

19

The term I_r was computed from the equation

$$I_r = K_1 e^{-K_2/T_r} \tag{7}$$

where T_r is the temperature of the reference target measured with the thermocouples. The Δi_{wr} is the difference in signal between the reference target and the point or points on the model where the temperature is to be measured. The wall temperature calculation is shown graphically in Fig. 13.

3.3.2 Data Reduction Procedure

The data for each reduction were in three logical parts: (1) tunnel data taken through the tunnel data system consisting of the tunnel parameters and oncenter line time codes; (2) infrared parameters, such as frame time codes and monitor sensitivity, taken through the tunnel data system during analog tape playback; and (3) the infrared data comprised of one or more digitized camera frames.

The first step in data reduction was the conversion of the raw counts to heat-transfer coefficients and this was accomplished in two parts. The first was the conversion of the counts to temperature in degrees - R using the count level of a reference point of known temperature in the camera frame, the emissivities of the model and the reference point, the monitor sensitivity, and constants obtained from the camera calibration curve. The second part consisted of converting temperatures to heat-transfer coefficients using a unique time for each point calculated from the frame time codes (the time the frame was recorded referenced to the model oncenter line time), certain electronic and physical delays, and the location of the point in the camera frame array.

The second step in the data reduction was the optional data compression. Frames may be reduced individually, or having obtained the heat-transfer coefficients as above, up to 20 frames may be compressed to eliminate some noise by averaging corresponding points in each frame.

The final step was the display of the results. This consisted of machine plots of heat transfer versus distance along model centerline rays, contour plots of lines of constant heat transfer, and tabulations of Stanton numbers and tunnel parameters.
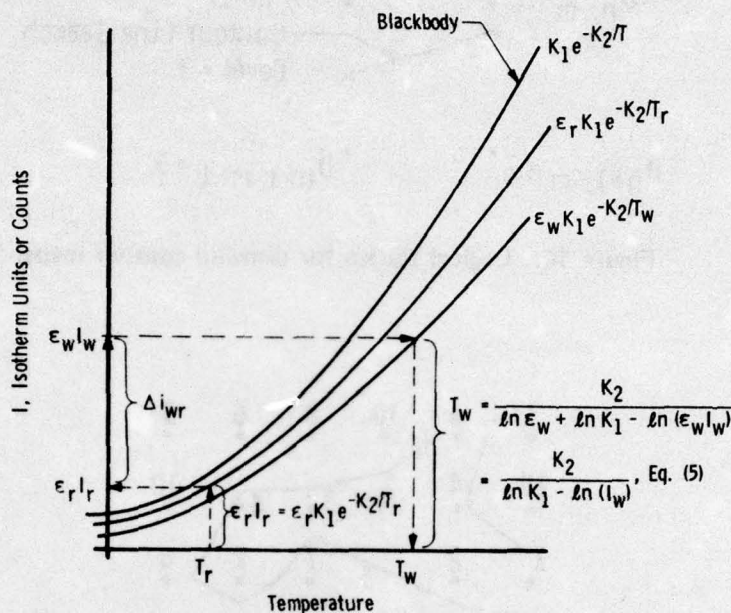
Figure 13. Graphical representation of wall temperature data reduction.

3.3.3 Contour Plots

Each contour plot is produced by a single pass through the array. First, the search levels are chosen as certain percentages of the maximum value on the model centerline. Successive rows, taken two at a time, are examined. Of these, successive points (taken two at a time) are examined. The resultant is four data points which form a logical square. Each of the sides of this square is examined by checking the data points which form the corners, to determine if any contour level will cross two sides. That is, if the value of the search level is between the value of any two data points then the contour line must pass between these two points. Linear interpolation is then employed to locate the exact location of the contour line between the data points. Each logical square is searched for all contour levels.

Figure 14 shows a single contour line drawn within one logical square. The contour search level was 3 and was located between data points $D_{n, m}$ and $D_{n+1, m}$, and $D_{n, m+1}$ and $D_{n+1, m+1}$. The points for the contour level were located by interpolation (marked by X) and were connected by a straight line. Figure 15 shows how one contour level within a data array might appear.
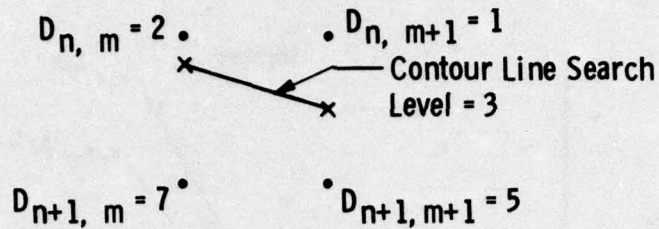
Figure 14. Logical square for drawing contour maps.

Search Level = 4.5
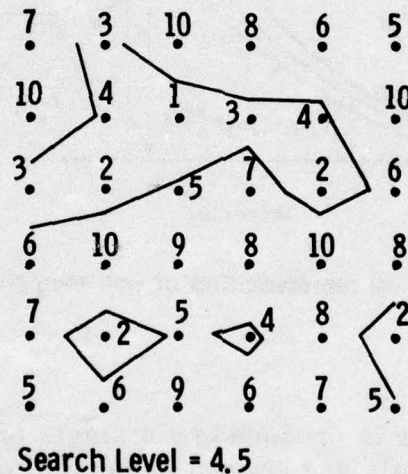
Figure 15. Contour lines in a data array.

4.0 RESULTS AND DISCUSSION

Typical data are shown in Figs. 16 through 24 (excluding Fig. 20). The basic plots and contour maps were computer produced. Model outlines, calculated values, and the explanatory callouts were added manually. Theory in all cases was computed by the methods of Refs. 9, 10, and 11 using the same conditions as those encountered during the test. Constant wall temperature was assumed for calculation of the theoretical result for the cone; however, measured values of wall temperature were used for the hemisphere-cylinder calculations.

Results from a run with a smooth cone are shown in Fig. 16. It was anticipated that this run would produce a fully laminar boundary-layer condition, and the data appear to indicate a laminar heating level. The heating distribution and level are in reasonably good agreement with the calculated values. Adding a boundary-layer trip (see Figs. 1 and 6) produced the significantly higher heating illustrated in Fig. 17. These data also agree very well with theoretical turbulent heating values. Free-stream Reynolds number was then adjusted to produce a transitional boundary layer and the resulting reduced infrared data are presented in Fig. 18. All the cone data shown in Figs. 16 through 18 show a region of apparent low heat transfer near the model base. This area corresponds to the metal inserts in the model surface (see Fig. 1). The lower emissivity and temperature of the metal as compared to the RTV-60 produced the indicated decrease in heat transfer.

A contour plot presented in Fig. 19 illustrates the heat-transfer distribution corresponding to the transitional boundary-layer case illustrated by the centerline distribution shown previously in Fig. 18. Since these data were obtained at zero angle of attack, the isotherms would be expected to appear as straight lines normal to the body axis. Although there may be some asymmetry in the transition pattern, these data show an apparent gradual change in heat transfer at the edge of the model from the lowest contour value to the higher ones.
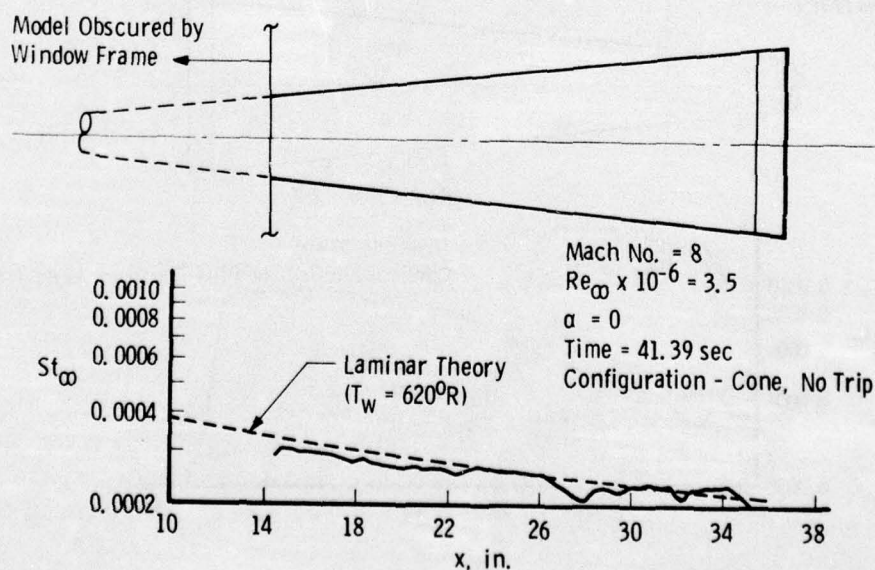
Figure 16. Longitudinal centerline heat-transfer distribution on a 6-deg cone with a laminar boundary layer.
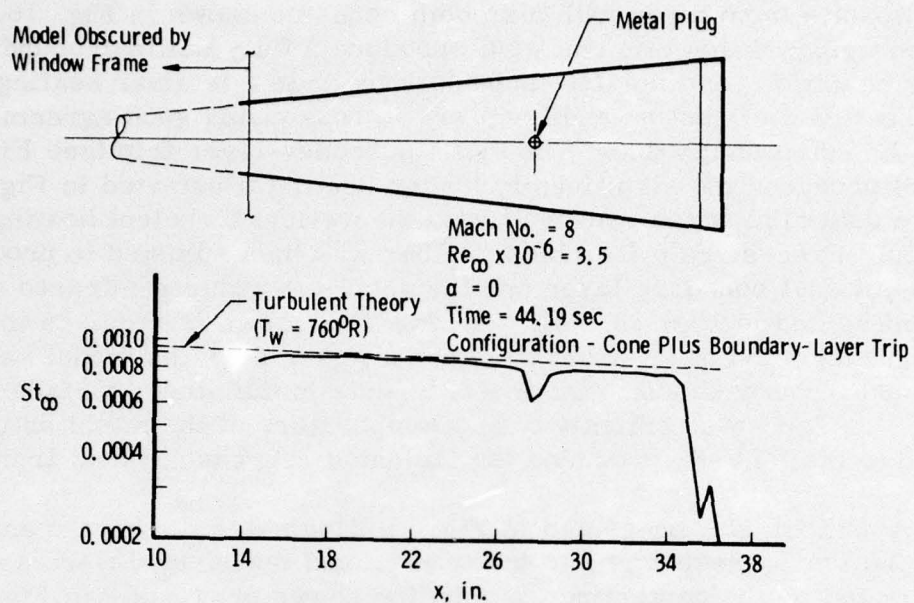
23

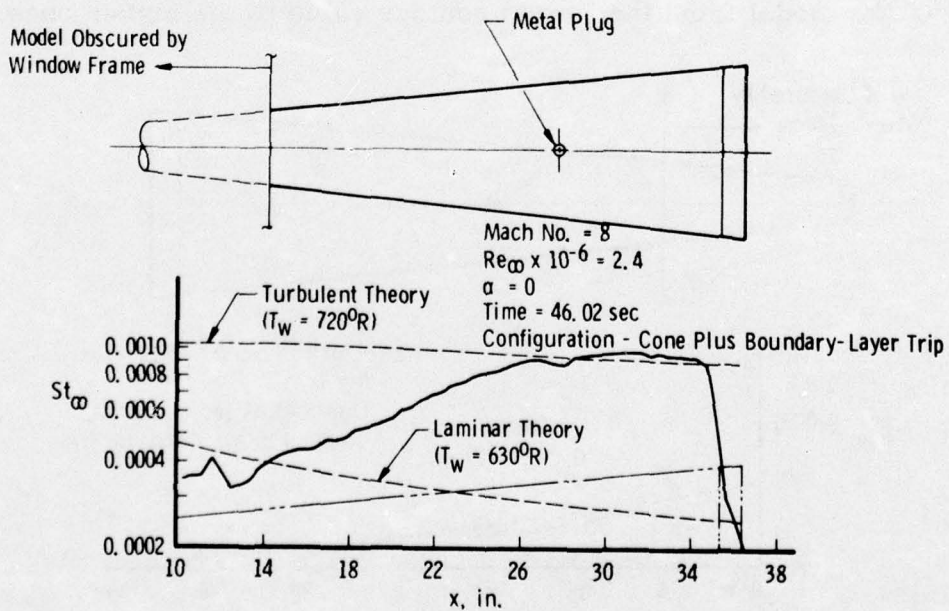**Figure 17. Longitudinal centerline heat-transfer distribution on a 6-deg cone with a turbulent boundary layer.**

Figure 18. Longitudinal centerline heat-transfer distribution on a 6-deg cone with a transitional boundary layer.

Mach No. = 8
$Re_\infty \times 10^{-6} = 2.4$
$\alpha = 0$
Time = 46.02 sec
Configuration - Cone Plus Boundary-Layer Trip
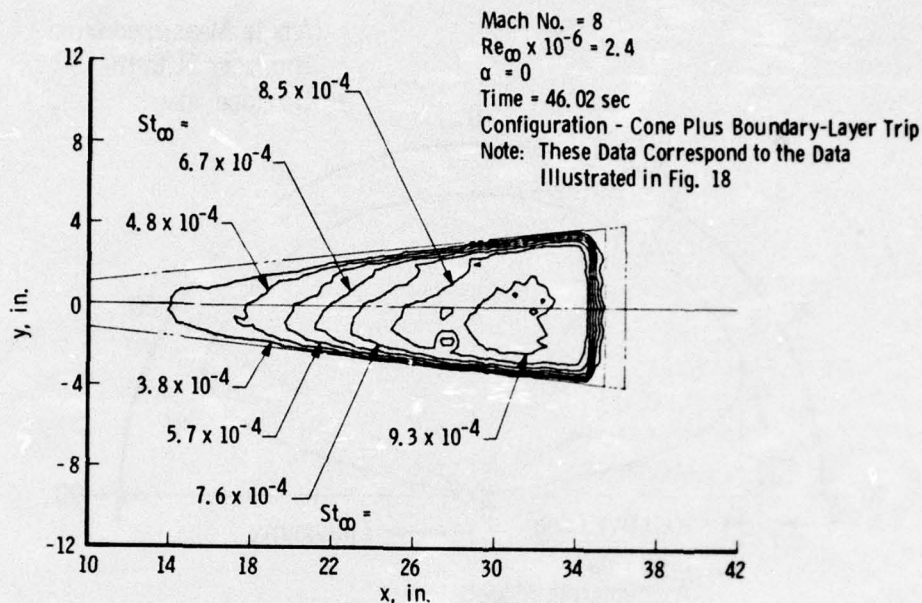Note: These Data Correspond to the Data
Illustrated in Fig. 18

Figure 19. Heat-transfer contour map of a 6-deg cone with a transitional
boundary layer.

This edge effect is caused by a combination of two characteristics
of the measurements. First, the camera will not provide a step change
in output signal when it scans across a step change in radiation (i.e.,
the model outline). This is attributable to the finite size of the camera's
signal detector imaged on the scene being scanned (instantaneous field
of view) and to the frequency response of the electronic circuits pro-
cessing the signal from the detector. The second characteristic is
the directional emittance of the model surface. Although the directional
emittance of the model material has not been measured, nonmetals
typically have the distribution shown in Fig. 20. In general, nonmetals
have a constant emissivity for angles of incidence measured from the
normal of 60 deg or less. Beyond 60 deg the value of emissivity falls
off rapidly. Regions on the model viewed with an angle of incidence
greater than 60 deg appear to be cooler than they actually are since
constant emissivity was assumed for data reduction. Table 1 gives
the estimated step response and the directional emittance effects
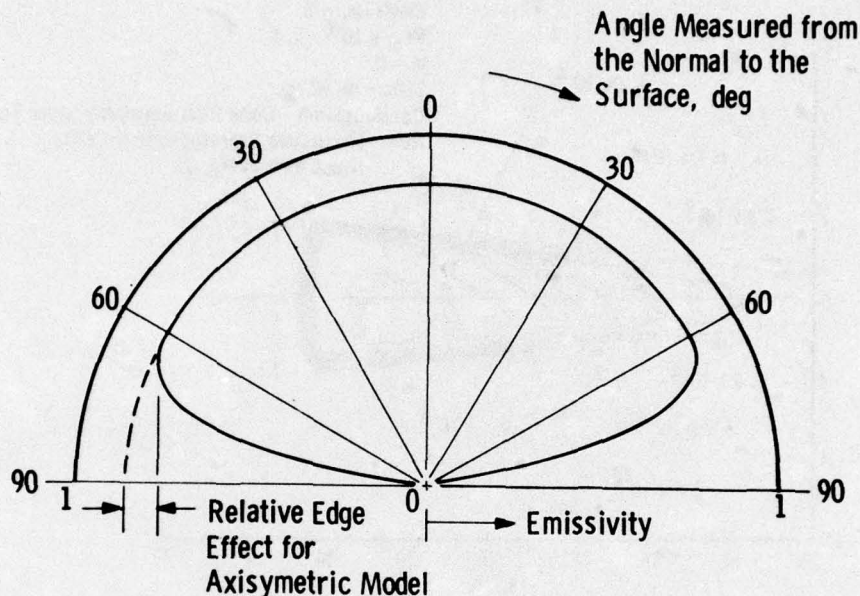applicable to the two models tested.

25

Figure 20. Directional emittance typical of nonmetals.

The hemisphere-cylinder data shown in Fig. 21 exhibit an intoler-
able amount of noise for the cylindrical portion of the model. The
source of the noise was traced to the magnetic tape system which
recorded the data in analog form. The peak-to-peak limits of the noise
contribution from the tape system are shown above and below the
Stanton number value of 3.5×10^{-4}. Because of the nonlinear rela-
tionship between Stanton number and the recorded analog signal, the
tape system noise contribution is negligible at the upper range of the
Stanton numbers. A significant reduction in the noise effects was
achieved by averaging the Stanton numbers from 20 consecutive frames.
The results are shown in Fig. 22. The averaging process should have
reduced the random noise by a factor of the reciprocal of the square
root of the number of samples and it apparently did. The high values
of Stanton number just aft of the model base are thought to be a result
of specular reflections of the radiation from the model sting. During
the test the window and mirror mounting tank (see Fig. 7), which are
not water cooled, reached a temperature near the IR window of 585°R.
The polished steel sting is believed to have reflected the radiation
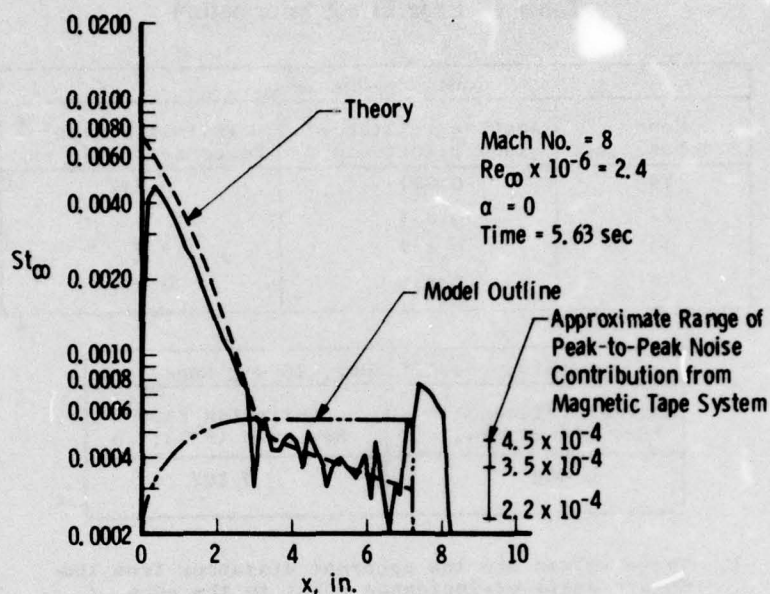from the tank into the camera.

26

Figure 21. Heat-transfer distribution along the centerline of a 3-in.-radius hemisphere-cylinder ~ single frame.
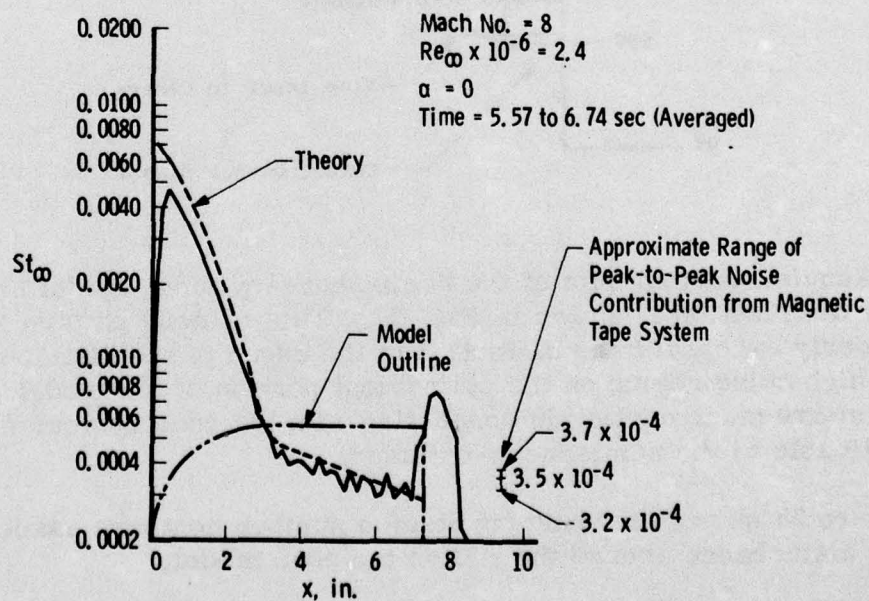

Figure 22. Heat-transfer distribution along the centerline of a 3-in.-radius hemisphere-cylinder ~ 20-frame average.

Table 1. Edge Effect Information

Cone, 25-deg Lens		
Cone Station, in.	Angular Emittance[1] Edge Effect, in.	Estimated Step[2] Response (95%), in.
14	0.221	0.247
22	0.334	
30	0.447	↓
36	0.531	0.247

Hemisphere-Cylinder, 10-deg Lens	
Angular Emittance[1] Edge Effect, in.	Estimated Step[2] Response (95%), in.
0.402	0.107

1. These values are the apparent distances from the 60-deg angle-of-incidence point to the edge of the model.

2. Step response based on manufacturer's instantaneous field-of-view data.
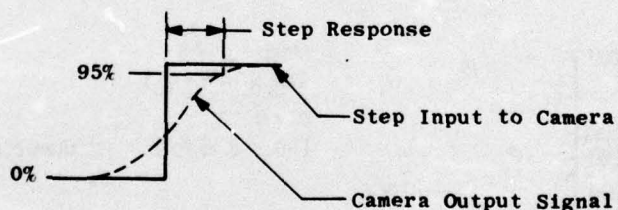
A planview contour plot of the hemisphere-cylinder model heat-transfer distribution is shown in Fig. 23. This contour pattern is very orderly except for the distortion at the edges of the distribution and the high noise region on the cylindrical portion of the model. All the comments made earlier in connection with the cone contour map are applicable to the hemisphere-cylinder.

Figure 24 shows the constant Stanton number contours associated with the disturbance around the rod on the cone model.

28

Mach No. = 8
Re∞ x 10⁻⁶ = 2.4
α = 0
Time = 5.57 to 6.74 sec (Averaged)
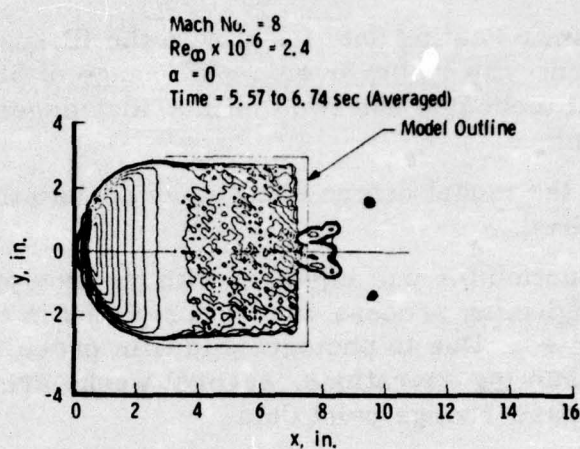
Figure 23. Heat-transfer contour map on a 3-in.-radius hemisphere-cylinder.

Mach No. = 8
Re∞ x 10⁻⁶ = 3.5
α = 0
Time = 27.32 sec
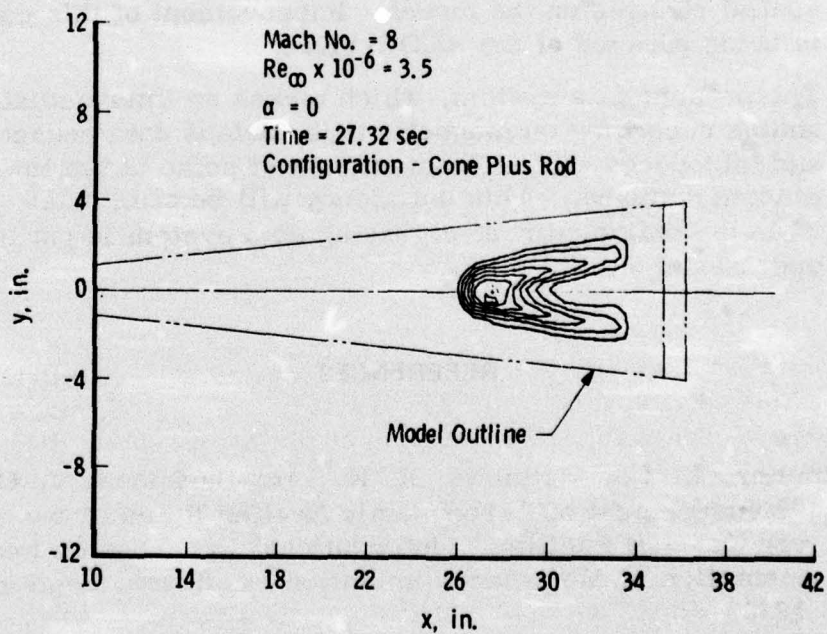Configuration - Cone Plus Rod

Figure 24. Heating contour map of area around rod in cone model.

29

5.0 CONCLUSIONS

The aerodynamic heating data taken with the IR system show excellent agreement with theory over a wide range of Stanton numbers. This experimental technique has two distinct advantages over the phase-change paint technique.

1. Painting the model before each injection into the flow is not required.

2. Data reduction for one injection with the exception of the offline digitizing process can be completed in approximately five minutes. Due to photographic film processing and other time consuming operations, several weeks are required to reduce phase-change paint data.

The two major deficiencies of the technique at this time are:

1. The spatial resolution of the camera is poorer than desired for taking data near the edge of the model or near step spatial changes on the model. Improvement of this condition is being pursued at the AEDC-VKF.

2. The present data system, which makes an intermediate analog recording on magnetic tape, delays data reduction and introduces a significant amount of noise at the low Stanton numbers. This deficiency will be eliminated when the online, direct-digitizing data system is put into operation.

REFERENCES

1. Trimmer, L. L., Matthews, R. K., and Buchanan, T. O. "Measurement of Aerodynamic Heating Rates at the AEDC von Karman Facility." International Congress on Instrumentation in Aerospace Simulation Facilities, September 1973.

2. Matthews, R. K. and Gilley, G. E. "Reduction of Photographic Heat-Transfer-Rate Data at AEDC." AEDC-TR-73-90 (AD762928), June 1973.

3. Baker, S. S. and Matthews, R. K. "Demonstration of the Thermographic Phosphor Heat-Transfer Technique as Applied to Aerodynamic Heating of External Stores." AEDC-TR-73-128, AFATL TR-73-154 (AD769306), November 1973.

4. Thomann, H. and Frisk, B. "Measurement of Heat Transfer with an Infrared Camera." International Journal of Heat and Mass Transfer, Vol. 11, Pergamon Press, 1968, pp. 819-826.

5. Schepers, H. J. "Heat Transfer Investigation of Axisymmetric Bodies at Hypersonic Speeds by Means of Infrared Measurements." NASA TTF-14,509 (A Translation of DLR-Mitt-71-19), August 1972.

6. Compton, Dale L. "Convective Heating Measurements by Means of an Infrared Camera." NASA TMX-2507, February 1972, pp. 645-660.

7. Hillsamer, Max E. "Correlation of Heat Transfer Data Obtained by the Infrared Scanner and Temperature Sensitive Coating Techniques." Air Force Flight Dynamic Laboratory AFFDL-TM-75-34-FXG.

8. Sivells, J. C. "Aerodynamic Design and Calibration of the VKF 50-Inch Hypersonic Wind Tunnels." AEDC-TDR-62-230 (AD299774), March 1963.

9. Patankar, S. V. and Spalding, D. B. Heat and Mass Transfer in Boundary Layers. C.R.C. Press, Cleveland, 1968.

10. Mayne, A. W., Jr., and Dyer, D. F. "Comparisons of Theory and Experiment for Turbulent Boundary Layers on Simple Shapes at Hypersonic Conditions." Proceedings of the 1970 Heat Transfer and Fluid Mechanics Institute, Stanford University Press, 1970.

11. Inouye, M., Rakich, J. V. and Lomax, H. "A Description of Numerical Methods and Computer Programs for Two-Dimensional and Axisymmetric Supersonic Flow Over Blunt-Nosed and Flared Bodies." NASA TN D-2970, August 1965.

NOMENCLATURE

c	Specific heat of model material, Btu/lbm-°R
C_p	Specific heat of test gas at constant pressure, Btu/lbm-°R
$D_{n, m}$; $D_{n+1, m}$; etc.	Data words in logical square
h	Heat-transfer coefficient, Btu/ft^2-sec-°R
I	Camera output, isotherm units or counts
Δi_{wr}	Difference in camera output between the model wall and the reference target, isotherm units or counts
K_1, K_2	First and second constants in camera output-temperature equation, isotherm units or counts, and °R respectively
k	Thermal conductivity of model material, Btu/ft-sec-°R
M	Mach number
P	Tunnel stagnation pressure, psia
Re	Reynolds number, per ft
St	Stanton number, see Eq. (2)
T	Temperature, °R
t	Time from start of heating, sec
V	Velocity, ft/sec
x	Distance from model nose, in.
y	Longitudinal distance from model centerline, in.
α	Angle of attack, deg
β	See Eq. (4)
ϵ	Emissivity integrated over the spectral band of the infrared camera
ρ	Density of the model material or free-stream density of the test gas, lbm/ft^3

SUBSCRIPTS

∞	Free-stream conditions
a	Ambient conditions
i	Initial conditions
o	Stagnation conditions
r	Reference
w	Model wall